Indian Journal of Chemistry
Vol. 58A, March 2019, pp. 313-320

Conversion of fructose into 5-hydroxymethylfurfural over mesoporous-ZrO_2-phosphomolybdic acid nanocomposite catalysts

Nayeem Pasha[a,*], P Krishna Kumari[b], N Vamsikrishna[a], N Lingaiah[b], N J P Subhashini[a] & Shivaraj[a,*]

[a]Department of Chemistry, Osmania University, Hyderabad 500 007, Telangana, India

[b]Catalysis Laboratory, Inorganic & Physical Chemistry Division, CSIR-Indian Institute of Chemical Technology, Hyderabad 500 007, Telangana, India

Email: nayeem77sk@gmail.com

Received 27 August 2018; revised and accepted 5 February 2019

A series of phosphomolybdic acid (MPA) with varying content, incorporated into the mesoporous zirconia (ZMPA) catalysts have been prepared by surfactant-assisted sol-gel copolymerization technique. These catalysts have been evaluated for selective dehydration of fructose to 5-hydroxymethyl furfural (HMF). The catalysts have been characterized by X-ray diffraction, nitrogen physisorption, Fourer-transform infrared spectroscopy, temperature programmed disorption, pyridine adsorbed FT-infrared spectroscopy and transmssion electron microscopy. The characterization results suggest that these catalysts possess ordered mesoporous structure with Keggin heteropoly molybdate. Moreover the incorporation of phosphomolybdic acid into mesoporous zirconia resulted in the generaton of more number of strong acidic sites. These catalysts exhibited about 80% HMF yield within 30 min of reaction time. The existence of relatively strong interactions between the MPA Keggin units with ZrO_2 mesoporous structure played a crucial role in fabricating the stable heterogeneous catalyst. This catalyst has been found to be reusable with constant activity.

Keywords: Fructose, Phosphomolybdic acid, 5-Hydroxymethylfurfural, Mesoporous zirconia

Renewable biomass resources are promising alternatives for sustainable supply of liquid fuels and chemicals. One of the top building-block chemicals derived from biomass is 5-hydroxymethylfurfural (HMF). It is a versatile intermediate for synthesis of fine chemicals, pharmaceuticals, plastic resins, fuels and etc[1-3]. It has been reported that HMF could be synthesised from fructose which is obtained directly from biomass or by isomerization of glucose. The study of catalytic dehydration of fructose into HMF has received considerable attention in recent times[4-6]. Many acid catalysts have been investigated for this important transformation, including mineral or organic acids, zeolites, metal ions, acidic ionic liquids, and acidic resins[7,8]. Homogenous acids show inherent drawbacks in product separation and equipment corrosion. Solid acids suffer from low catalytic performance as well as long reaction times. In the case of acidic resins, reaction temperature is strictly limited due to their thermal stability. Therefore, developing more environmental friendly and active solid acid catalysts to replace the liquid acid catalysts is highly desired[9-12].

Heterogeneous catalysts may provide an efficient methodology for biomass conversion allowing for high reaction rates and selectivity of the target products. The catalytic conversion of biomass to promising chemicals over solid catalysts has received much attention in recent years[13-15]. Heteropolyacids (HPA) are known to be active catalysts for many acid catalyzed reactions. HPAs have proved to be one of the alternatives to traditional acid catalysts due to their strong acidity, as they possess readily available protons in their Keggin structure. HPAs are widely used as catalysts in a number of homogeneous, heterogeneous acid and redox type catalytic reactions, due to their specific physicochemical properties such as high acidity and oxidizing properties[16]. The major disadvantages of HPA as catalyst lie in their low thermal stability and low surface area. HPAs supporting on acidic supports not only enhance acidity but also thermal stability. Moreover, HPAs can be made insoluble by supporting them on solid support. The support provides an opportunity for HPAs to be dispersed over a large surface area, which results in increased catalytic activity. Various supports like silica[17,18], titania[19,20], active carbon[21],

niobia[22,23], zirconia[24,25], alumina[26], MCM-41[27,28] and acidic ion exchange resins[29] have been used for supporting HPAs.

Zirconia (ZrO_2) has received considerable attention because of its semiconducting properties, high thermal stability, reducing character and acid-base bifunctional nature[30,31]. Owing to these features, zirconia-based materials are potentially applicable in redox and photo-catalysis. Recent studies have indicated that mesoporous zirconia is suitable for supporting HPA anions via relatively strong chemical bonds[32-34]. HPA clusters immobilized on ZrO_2 can exhibit strong acid and redox character[35]. The objective of the present study is to prepare mesoporous-ZrO_2-phosphomolybdic acid nano composites by a one pot method and evaluate their catalytic performance in selective conversion of fructose into HMF. The relation between composite surface-structure characterizations with that of fructose dehydration activity has been studied. The optimization of reaction parameters such as catalyst weight, reaction temperature, time and reusability of catalyst is also one of the aims of the present study.

Materials and Methods

Preparation of mesoporous ZrO_2-MPA nanocomposites

Mesoporous zirconia and its MPA composites were prepared according to a reported method[36]. In a typical synthesis, 0.5 g of Pluronic F127 (Sigma Aldrich) was dissolved in anhydrous ethanol (SD Fine Chem Limited) until it formed a clear solution. Then, a 1.6 g of $ZrOCl_2.8H_2O$ (Sigma-Aldrich) was added to the surfactant solution and the mixture was stirred vigorously for 2 h at room temperature. After this, a clear solution of MPA (Sigma Aldrich) in ethanol was added drop wise and the resulting mixture was stirred at room temperature for another 10 min. The homogeneous solution underwent solvent evaporation at 40 °C for 3 days and the foam-like product was dried at 100 °C under vacuum for 12 h. The template was removed by step wise calcinations with a heating rate of 0.5 °C min^{-1} at 250 °C for 4 h and then, at 350 °C for 2 h in air. The resultant solid product was designated as ZMPA (*w*), where *w* represents the percentage weight of MPA.

Characterization of catalysts

X-Ray powder diffraction patterns were recorded on Ultima-IV (M/s. Rigaku Corporation, Japan) XRD unit operated at a voltage of 40 kV and current of 40 mA equipped with nickel-filtered Cu-Kα radiation (λ = 1.54056 Å).

The acidity of the catalysts was measured by temperature programmed desorption of ammonia (TPD–NH_3). In a typical experiment, 0.1 g of catalyst was loaded and pre-treated in helium atmosphere at 300 °C for 2 h. After pre-treatment, the temperature was brought to 100 °C and the adsorption of NH_3 was carried out by passing a mixture comprising 10% NH_3 and 90% He over the catalyst for 1 h. The catalyst surface was then flushed with He, at 100 °C for 2 h to flush off the physisorbed NH_3. Thereafter, TPD of NH_3 was carried with a temperature ramp of 10 °C/min and the desorbed ammonia was monitored using a thermal conductivity detector (TCD) of a gas chromatograph.

The FT-IR spectra were recorded on a Shimadzu (IR Prestige-21) infrared spectrometer using the KBr pellet method in the wave number range of 4000–400 cm^{-1}, with a resolution of 4 cm^{-1} at room temperature. The pyridine adsorbed FT-IR patterns were recorded in the diffuse reflectance infra-red Fourier transform (DRIFT) mode. In the characteristic experiment, the sample is degassed under vacuum at 200 °C for 3 h followed by suspending dry pyridine. Then, the sample is heated at 120 °C for 1 h, and then the spectra of the pyridine-adsorbed sample are recorded at room temperature.

Transmission electron microscopy (TEM) was performed using a Phillips TEM CM 200 fitted with a LaB_6 filament, operating at 200 kV. The samples were first softly powdered, than ultrasonicated in ethanol and a drop was placed onto the carbon coated copper grid, the solvent was then evaporated in an air oven at 80 °C for 6 h.

The morphological analyses were performed on a JEOL JSM-6360LV scanning electron microscope (SEM) equipped with an INCA EDX energy dispersive X-ray (EDX) spectroscopy detector. Data acquisition was performed with an accelerating voltage of 20 kV and 60 s accumulation time.

The surface areas were calculated from the Brunauer–Emmett–Teller (BET) equation and pore size distributions were calculated using the Barrett–Joyner–Halenda (BJH) model from the adsorption branch of the isotherms carried out at −196 °C on a Quadrasorb-SI analyzer (M/s. Quantachrome Instruments, USA). Prior to the measurement, the samples were degassed at 150 °C for 1 h to remove pre-adsorbed gases.

Fructose dehydration procedure

Fructose dehydration was performed in a 15 mL sealed tube. In a typical experiment, 0.36 g of fructose

dissolved in 5 mL of dimethyl sulfoxide (DMSO) and 50 mg of catalyst was added. The mixture was heated at 120 °C for 30 min, under autogenous pressure. After the reaction, the mixture was filtered and then decanted into a volumetric flask using water as diluent, and the product was analyzed by HITACHI-HPLC system equipped with binary 2130 pumps, a manual sampler, and 2490 refractive index detector, maintained at 50 °C. The products were separated in a sugar column (250×4.8 mm) ion-exclusion column, maintained at 60 °C using water as the mobile phase with 0.8 mL/min flow rate.

Results and Discussion

Catalyst characterization

Powder X-ray diffraction patterns:

The low angle X-ray diffraction patterns of the meso-ZrO_2 and ZMPA (*w*) samples are shown in Fig. 1a. A weak and broad reflection in low-angle range could be observed for all samples. These peaks indicated the 100, 110, 200 Bragg reflections of hexagonal *p6mm* structural arrangement. The broadening of the main diffraction peaks of ZPMA (*w*) related to the mesoporous zirconia. The $d_{(100)}$ and unit cell parameter values are shown in Table 1, and they are in concurrence with earlier reports[35]. These results indicate the presence of mesoporous structure in all the ZMPA (*w*) samples. In Fig. 1b, the wide-angle X-ray diffraction patterns of meso-ZrO_2 and ZMPA (*w*) samples showed several weak diffraction peaks in the 2θ range of 30–75º, which were related to the reflections of tetragonal ZrO_2 phase (ICDD No. 88-1007). The determination of the crystallite size of ZrO_2 is quite complicated but the nano-crystalline nature of the tetragonal ZrO_2 was evidenced by the broadness in the peaks[37,38]. From the wide angle XRD patterns, it could be observed that there are no diffraction signals corresponding to heteropoly acid. It means the heteropoly acid MPA is in highly dispersed form or below the detection limit (~4 nm) of XRD. Unifying both these results, the ZrO_2-phosphomolybdic acid catalysts are termed as nanocomposite catalysts.

Nitrogen physisorption

In order to understand the pore structure of the catalysts, the N_2 adsorption-desorption measurements were carried out. The adsorption isotherms of the samples are shown in Supplementary Data, Fig. S1a. The obtained isotherms are almost similar for all samples which could be identified as type IV according to the IUPAC classification. The H_1 and H_2

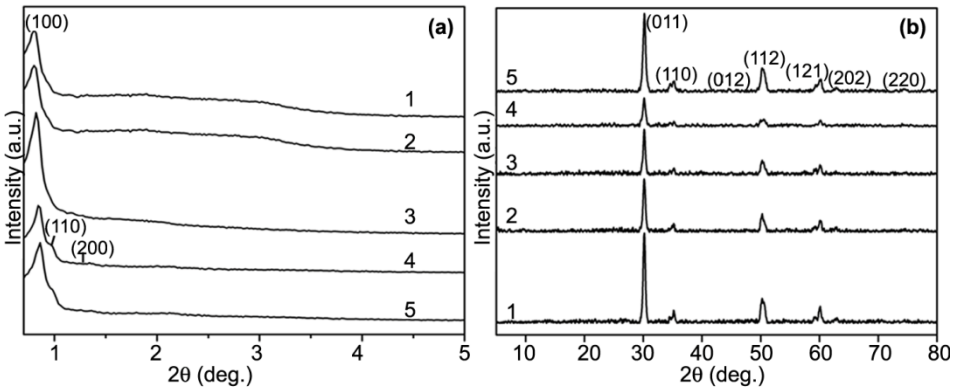

Fig. 1 — (a) Small angle XRD patterns and (b) wide angle XRD patterns of meso-ZrO_2 and ZMPA samples (meso-ZrO_2 (1), ZMPA (20) (2), ZMPA (25) (3), ZMPA (30) (4), and, ZMPA (35) (5)).

Table 1 — Surface and bulk properties of mesoporous zirconia (meso-ZrO_2) and ZMPA (*w*) composites

Sample	[a]Surface area (m^2/g)	[b]Pore (cc/g^{-1})	[c] Pore size (nm)	[d]d_{100} (nm)	[e]Unit cell (nm)	[f]WT (nm)
Meso-ZrO_2	77.6	0.08	5.6	11.0	12.7	7.1
ZMPA (20)	15.5	0.05	5.2	10.9	12.5	7.3
ZMPA (25)	20.3	0.03	5.0	10.7	12.3	7.3
ZMPA (30)	30.4	0.02	4.6	10.4	12.0	7.5
ZMPA (35)	32.6	0.02	4.5	10.2	11.7	7.2

[a]BET surface area, [b] total pore volume at relative pressure p/p_0, [c]average pore size, [d]periodicity,[e]unit cell parameter $=2^{½}\,d(110)$,[f]pore wall thickness WT = $(3^{½}\,a_0/2\,)$-D.

type hysteresis behaviour of the samples, suggest the characteristic of mesoporous materials with well-defined cylindrical pores[39]. The capillary condensation was observed for the samples within the P/P_o range of ~0.6–0.8 which is the characteristic feature for the mesoporous materials. The textural properties of the samples are also summarized in Table 1. The mesoporous zirconia has BET surface area of 77 $m^2 g^{-1}$ and a pore volume of 0.08 $cm^3 g^{-1}$. While mesoporous ZPMA composites were found to have lower BET surface areas in the range 15.5–32.6 $m^2 g^{-1}$ with the pore volume in the range of 0.02–0.05 $cm^3 g^{-1}$. The mesopore diameter significantly decreased after MPA incorporation in the parent mesoporous zirconia due to the deposition of MPA inside the mesopores. The pore size distribution calculated from the adsorption data based on the non-local density function theory (NLDFT) analysis of the adsorption branches of meso-$ZrO_2$and ZMPA (*w*) composites revealed quite a narrow distribution of pore sizes. The pore size distributions of the samples shown in Fig. S1b exhibit an average pore size of 4.5–5.6 nm. This is a characteristic feature of mesopores and confirms the presence of uniform mesopores in the present samples.

Fourier transform-infrared (FT-IR) spectroscopy:

The FT-IR spectra of pure MPA, meso-ZrO_2 and ZMPA samples are shown in Fig. 2. The absorption bands at 1068, 957, 880 and 756 cm^{-1} could be attributed to the presence of P–O, Mo=O, Mo−O_b–Mo and Mo−O_c–Mo, of Keggin MPA respectively[36,40]. All the ZMPA samples exhibited these typical bands similar to those of parent MPA, indicating the retention of Keggin structure even after the incorporation of MPA in meso-ZrO_2. In addition, a shift in ν_{as} Mo=O of MPA from 957 cm^{-1} to 943 cm^{-1} in ZMPA (*w*) samples represents the strong interaction between zirconia and terminal oxygen of Mo=O, leading to lower wave numbers. Further, the presence of distorted PO_4 central units could be indicated by the intense band at 1192 cm^{-1} of P–O stretching mode, suggesting the strong interaction.

Temperature programmed desorption of ammonia:

The strength and number of surface acidic sites of the samples were investigated by NH_3-TPD technique. Based on the desorption temperature of NH_3, the strength of acidic sites are classified into weak acidic sites (<250 °C), medium (250–400 °C), and strong acidic sites (>400 °C) [41] (results presented in Table 2). The synthesized meso-ZrO_2 and ZMPA (*w*) samples showed a broad desorption peak (not shown here). All the samples showed broad desorption peak at low temperature in the range of 150–250 °C, which corresponds to weak acid sites. In addition, ZMPA (*w*) nanocomposite samples showed desorption peaks at 350 to 450 °C and 550 to 650 °C, which can be attributed to the medium and strong acid sites, respectively. Dispersion of MPA into meso-ZrO_2 framework resulted in a notable increase in the number of acid sites. These results clearly indicate the formation of a large number of acid sites in ZMPA (*w*) nanocomposites. This is probably due to the effect of high dispersion of MPA in meso-ZrO_2 framework[42].

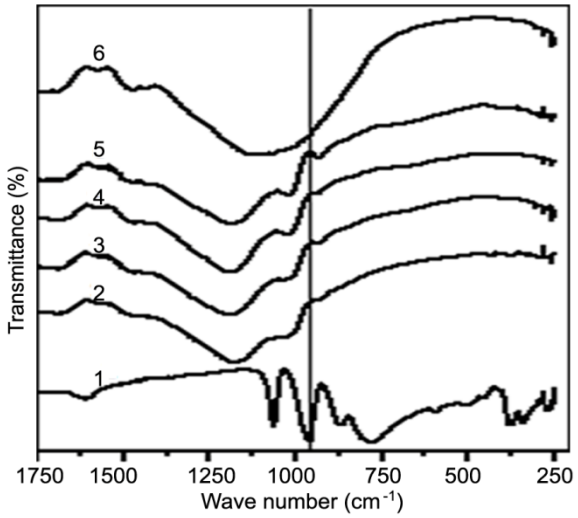

Fig. 2 — FT-IR patterns of meso-ZrO_2 and ZMPA samples (bulk MPA (1), ZMPA (20) (2), ZMPA (25) (3), ZMPA (30) (4), ZMPA (35) (5), and, meso-ZrO_2 (6)).

Table 2 — Acid strength distribution of Meso-Zro_2 and ZMPA (*w*) catalysts

Sample	Acidity (mmol/g)			Total acidity
	Weak	Moderate	Strong	
Meso-ZrO_2	0.313	0.804	0.484	1.601
ZMPA (20)	0.283	0.451	1.191	1.926
ZMPA (25)	0.297	0.482	1.397	2.181
ZMPA (30)	0.249	0.756	1.670	2.671
ZMPA (35)	0.250	0.603	2.501	3.354

Pyridine IR spectra

The pyridine-IR spectra were employed to evaluate the types of acidic sites in meso-ZrO_2 and ZMPA (*w*) samples. The FT-IR profiles are shown in Fig. 3. All the samples exhibited bands at 1441 and 1586 cm^{-1} demonstrating the existence of Lewis acid sites in the samples. The bands present at 1534 and 1640 cm^{-1} were the characteristic bands of pyridinium ion bonded to Brønsted acid sites. In addition, the band present at 1485 cm^{-1} was ascribed to both Brønsted and Lewis acid sites[43]. These results indicated that both Brønsted and Lewis acid sites existed in meso-ZrO_2 and ZMPA (*w*) samples. The Brønsted acidity enhanced with the increase of the MPA content; indicating that the introduction of MPA species improved the Brønsted acidity of ZMPA (*w*) samples. The improved Brønsted acidity might be due to the highly dispersed MPA species on ZrO_2.

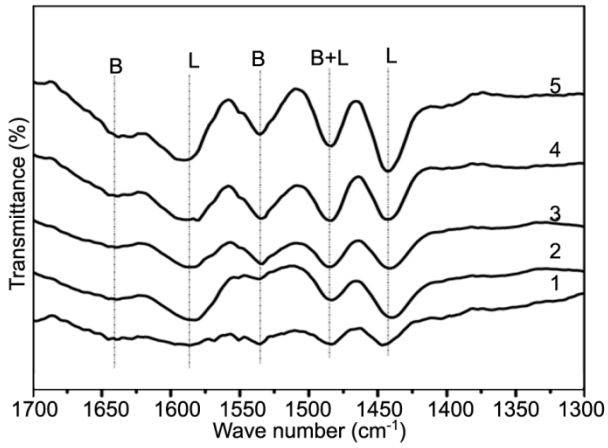

Fig. 3 — Pyridine FT-IR spectra of ZMPA samples (meso-ZrO_2 (1), ZMPA (20) (2), ZMPA (25) (3), ZMPA (30) (4), and, ZMPA (35) (5)).

TEM analysis

The TEM image of meso-ZrO_2 and ZMPA (*w*) samples is given in Fig. 4. TEM analysis shows an average inter pore distance of ~12.7, 12.5 and ~12.0 nm for meso-ZrO_2, ZMPA (20) and ZMPA (30) samples respectively. The *d*-spacing corresponding to the diffraction rings of the select-area electron diffraction (SAED) patterns which are in good agreement with the tetragonal crystal structure of ZrO_2.

Catalytic activity studies

Effect of MPA loading

The performances of the catalyst were investigated for the dehydration of fructose into 5-hydroxymethyl furfural (Scheme 1) and the results are presented in

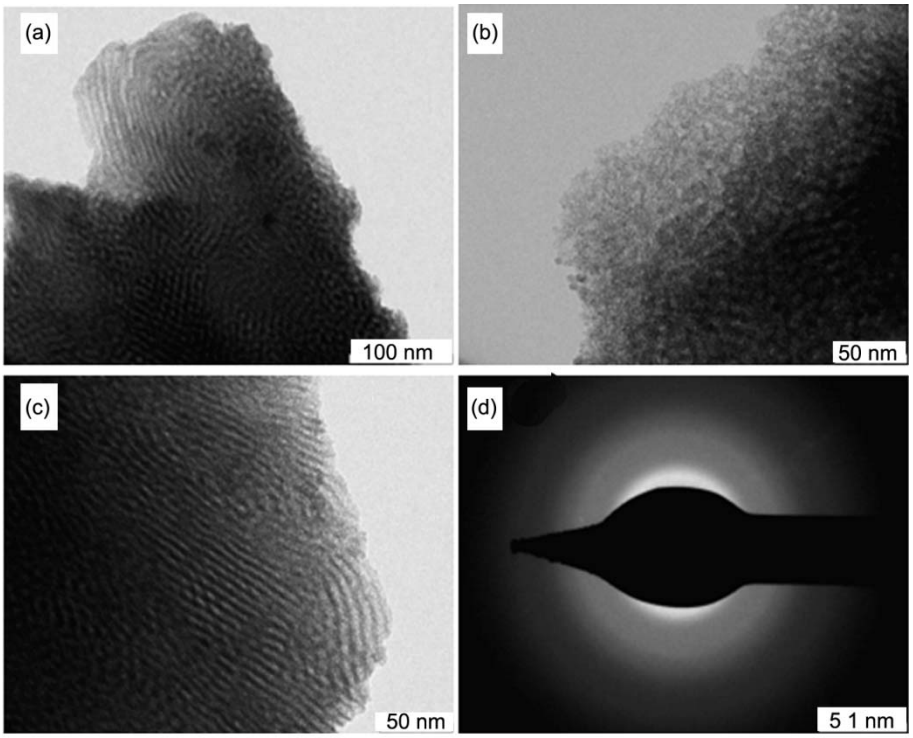

Fig. 4 — TEM images of (a) meso-ZrO_2, (b)ZMPA (20), (c) ZMPA (30), and, (d) SAED of meso-ZrO_2.

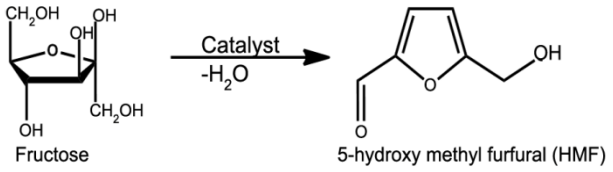

Dehydration of fructose to 5-hydroxy methyl furfural

Scheme 1

Supplementary Data, Fig. S2. Mesoporous-ZrO_2 exhibited about 29% HMF yield. While the catalytic activity of ZMPA composites showed higher yields towards HMF. ZMPA (30) catalyst showed a HMF yield of 52% and as the loading of MPA increased on ZrO_2, the yield of the HMF increased from 52 to 80.3%. Further, increase in MPA loading to ZMPA (35) the yield of the HMF decreased to 71%. The remarkable increase in activity from the 20 to 30 wt% of MPA on ZrO_2, might be due to the well dispersed MPA on zirconia, which resulted in the increase in acidity. XRD results clearly (Fig. 1b) suggested the well dispersed MPA on meso-ZrO_2 as XRD patterns associated to MPA Keggin ion were absent. These activity results can be ascribed due to the difference in acidic functionality. The 25 and 30% ZMPA samples showed acidity values as 2.18 and 2.67 mmol respectively and this acidity might be responsible for increase in the yield of HMF. The increased acidity of ZMPA (35) catalyst promotes the formation of side levulinic acid, resulting in a decrease in the yield of HMF.

Effect of reaction temperature

As the ZMPA (30) sample demonstrated the highest catalytic activity, it is selected and studied to optimise reaction conditions. The effect of reaction temperature on the dehydration of fructose to HMF was examined within the temperature range of 80 to 140 °C over ZMPA (30) catalyst and the results are presented in Fig. S3. The reaction temperature played a significant role on HMF yield. At 80 °C of reaction temperature, the yield of HMF is only 10%. As the temperature increased up to 120 °C, the yield increased up to a maximum of 80.3%. When the reaction temperature increased further to 140 °C, the yield of HMF decreased to 70%. The decrease in the yield might be due to further hydrolysis of HMF. Hence, it can be suggested that the maximum selectivity to HMF could be obtained at 120 °C over the present catalyst.

Effects of reaction time

The influence of reaction time on the yield of HMF catalyzed by ZMPA (30) is shown in Fig. S4. The yield of HMF increased gradually from 10 min to 30 min. The increase in reaction time improved the yield of HMF. The maximum HMF yield of 80.3% was obtained within 30 minutes. This indicates that the present catalyst is highly active as it showed high activity within short reaction time. On prolonged reaction time, the yield of HMF is decreased due to the degradation of HMF. These results are in support with earlier reports[44].

Effect of catalyst amount

The influence of catalyst weight on the dehydration of fructose to HMF was studied over ZMPA (30) catalyst and the results are presented in Fig. S5. The yield of HMF gradually increased from 20 to 80.3% as the catalyst amount increased from 10 to 50 mg. The enhancement in the yield with increase in catalyst amount might be due to increase in the accessibility and number of active sites in the reaction mixture. Further increase in catalyst amount to 75 mg, results in a drop in HMF yield to 63%. This suggests that the excess catalyst might be promoting polymerization of HMF[45]. These results indicate that 50 mg of catalyst amount is enough to attain the maximum yield of HMF.

Recycling of catalyst

ZMPA (30) catalyst efficiency and stability were investigated by conducting recycling experiments under optimized reaction conditions and the results illustrated in Fig. S6. After the completion of the reaction, the catalyst was recovered by centrifugation, thoroughly washed with ethanol and dried in an oven at 100 °C and used for the next cycle. The catalyst retained the catalytic activity even after five cycles with a slight decrease in the yield of the HMF from 80.3% to 75% after the fifth cycle.

The spent catalyst was characterized by SEM-EDX and IR spectroscopy. These results showed no change in the morphology and stability of Keggin structure of the used catalyst. The FT-IR spectrum showed the characteristic of Keggin structure of the 12-phosphomolybdic acids (Fig. S7). These results clearly support the high durability of the ZMPA (30) catalyst under the present reaction conditions. The catalytic activity of the ZMPA catalysts was compared with the reported catalytic systems and presented in Table 3.

Table 3 — Comparison of different reported catalysts with ZMPA (30) catalyst

Catalyst	Reaction temperature (°C)	Time (h)	Fructose conversion (%)	HMF Yield (%)	Ref.
$SO_4^{2-}/ZrO_2–Al_2O_3$	130	4	99	57	46
Nafion	120	4	94	75	47
Amberlyst-15	120	4	100	76	47
H-BEA zeolite	120	4	100	51	47
ZMPA (30)	120	0.5	100	80.3	Present work

Conclusions

Meso-ZrO_2 and phosphomolybdic acid containing mesoporous ZrO_2 nanocomposites were successfully prepared and systematically characterized. The incorporation of MPA into the meso-ZrO_2 resulted in the enhancement in acidity with accessible active sites. NH_3-TPD and Py-IR spectroscopy reveal that the strength and nature of acidic sites varied with change in MPA content on ZrO_2. The sample with ZMPA (30) is the optimum catalyst for fructose dehydration to HMF. Under the optimized conditions, ZMPA (30) catalyst showed complete conversion of fructose with 80.3% yield of HMF. The catalyst is reusable with constant activity.

Supplementary Data

Supplementary data associated with this article are available in the electronic form at http:// www.niscair.res.in/jinfo/ijca/IJCA_58A(03) 313-320_SupplData.pdf

Acknowledgement

NP gratefully thanks SERB-DST, New Delhi, for awarding Start-Up Research Grant (Young Scientists) Grant No.SB/FT/CS-074/2014.

References

1 Tian C, Bao C, Binder A, Zhu Z, Hu B, Guo Y, Zhao B & Dai S, *Chem Comm,* 49 (2013) 8668.
2 Huber G W, Chheda J N, Barrett C J & Dumesic J A, *Science,* 308 (2005) 1446.
3 Kunkes E L, Simonetti D A, West R M, Serrano-Ruiz J C, Gärtner C A & Dumesic J A, *Science,* 322 (2008) 417.
4 Nikolla E, Román-L Y, Moliner M & Davis M E, *ACS Catal,* 1 (2011) 408.
5 Nakajima K, Baba Y, Noma R, Kitano M, Kondo J N, Hayashi S & Hara M, *J Am Chem,* 133 (2011) 4224.
6 Shi C, Zhao Y, Xin J, Wang J, Lu X, Zhang X & Zhang S, *Chem Comm*, 48 (2012) 4103.
7 Van P R J, van der Waal J C, de Jong E, Rasrendra C B, Heeres H J & de Vries J G, *Chem Rev,* 113 (2013)1499.
8 Rosatella A A, Simeonov S P, Frade R F M & Afonso C A M, *Green Chem,* 13 (2011) 754.
9 Chen J, Li K, Chen L, Liu R, Huang X & Yeb D, *Green Chem*, 16 (2014) 2490.
10 Alamillo R, Crisci A J, Gallo J M, Scott S L & Dumesic J A, *Angew Chem Int Ed,* 52 (2013) 10349.
11 Yang Z Z, Deng J, Pan T, Guo Q X & Fu Y, *Green Chem,* 14 (2012) 2986.
12 Liu R L, Chen J Z, Huang X, Chen L M, Ma L L & Li X J, *Green Chem*, 15 (2013) 2895.
13 Shaal M G A, Dzierbinski A & Palkovits R, *Green Chem,* 16 (2014) 1358.
14 Egeblad K, Hansen J R, Marsden C C, Taarning E & Christensen C H, *Catalysis: The Royal Society of Chemistry,* 21 (2009) 13.
15 Ruppert A M, Weinberg K & Palkovits R, *Angew Chem Int Ed*, 51 (2012) 2564.
16 Kumar C R, Rambabu N, Lingaiah N, Sai Prasad P S & Dalai A K, *Appl Catal A Gen,* 471(2014) 1.
17 Dias J A, Caliman E, Dias S C L, Paulo M & de Souza A T C P, *Catal Today,* 85 (2003) 39.
18 Kamiya Y, Ooka Y, Obara C, Ohnishi R, Fujita T, Kurata Y, Tsuji K, Nakajyo T & Okuhara T, *J Mol Catal A Chem,* 262(2007) 77.
19 Kumbar S M, Shanbhag G V, Lefebvre F & Halligudi S B, *J Mol Catal A Chem,* 256 (2006) 324.
20 Damyanova S & Fierro J L G, *Chem Mater,* 10 (1998) 871.
21 Pizzio L R, Cacares C V& Blanco M N, *Appl Catal A Gen,* 167 (1998) 283.
22 Balaraju M, Nikhitha P, Jagadeeswaraiah K, Srilatha K, Sai Prasad P S & Lingaiah N, *Fuel Process Technol,* 91 (2009) 249.
23 Srilatha K, Lingaiah N, Prabhavathi Devi B L A, Prasad R B N, Venkateswar S & Sai Prasad P S, *Appl Catal A Gen,* 365 (2009) 28.
24 Mallik S, Parida K M & Dash S S, *J Mol Catal A Chem,* 261 (2007) 172.
25 Devassy B M & Halligudi S B, *J Catal,* 236 (2005) 313.
26 Sharma P, Vyas S & Patel A, *J Mol Catal A Chem,* 214 (2004) 281.
27 Kamalakar G, Komura K & Sugi Y, *Appl Catal A Gen,* 310 (2006) 155.
28 Rajasekar K & Pandurangan A, *Catal Comm,* 8 (2007) 635.
29 Baba T & Ono Y, *Appl Catal,* 22 (1986) 321.
30 Yamaguchi T, *Catal Today,* 20 (1994) 199.
31 Kaspar J, Fornasiero P & Hickey N, *Catal Today,* 77 (2003) 419.
32 Trolliet C, Coudurier G & Vedrine J C, *Top Catal,* 15 (2001) 73.
33 Pizzio L, Vázques P, Cáceres C & Blanco M, *Catal Lett,* 77 (4) (2001) 233.
34 Sharma P & Patel A, *Appl Surf Sci,* 255 (2009) 7635.

35 Salinas E L, Cortez J G H, Cortez M, Navarrete J, Yanos M, Vazquez A, Armendaris H & Lopez T, *Appl Catal,* 175 (1998) 43.
36 Armatas G S, Bilis G & Louloudi M, *J Mater Chem,* 21 (2011) 2997.
37 Garvie R C, *J Phys Chem,* 82 (1978) 218.
38 Shukla S & Seal S, *J Phys Chem B,* 108 (2004) 3395.
39 Kleitz F, Solvyov L A, Anil kumar G M, Choi S H & Ryoo R, *Chem Comm,* (2004) 1536.
40 Essayem N, Holmqvist A, Gayraud P Y, Vedrine J C & Ben T Y, *J Catal,* 197 (2001) 273.
41 Delannay F, *Characterization of Heterogeneous Catalysts* (Marcel Dekker, New York, USA) (1984).
42 Kim T, Burrows A, Kiely C J & Wachs I E, *J Catal,* 246 (2007) 370.
43 Miao Z, Song H, Zhao H, Xu L & Chou L, *Catal Sci Technol,* 4 (2014) 838.
44 Liu R, Chen J, Huang X, Chen L, Ma L L & Li X, *Green Chem*, 15 (2013) 2895.
45 Raveendra G, Srinivas M, Pasha N, Prasada Rao A V, Sai Prasad P S & Lingaiah N, *Reac Kinet Mech Cat*, 115 (2015) 663.
46 Yan H, Yang Y, Tong D, Xiang X & Hu C, *Catal Comm,* 10 (2009) 1558.
47 Shimizu K I, Uozumi R & Satsuma A, *Catal Comm,* 10 (2009) 1849.